

PREPARED FOR SUBMISSION TO JHEP

Using rates to measure mixed modulus-anomaly mediated supersymmetry breaking at the LHC

J. A. Conley,^a H. K. Dreiner,^a L. Glaser,^b M. Krämer,^b and J. Tattersall^{a,b}

^a*Physikalisches Institut der Universität Bonn
Nussallee 12, D-53115 Bonn, Germany*

^b*Institute for Theoretical Particle Physics and Cosmology
RWTH Aachen, D-52056 Aachen, Germany*

E-mail: conley@th.physik.uni-bonn.de, dreiner@th.physik.uni-bonn.de,
Lisa.Glaser@physik.rwth-aachen.de, mkraemer@physik.rwth-aachen.de,
jamie@th.physik.uni-bonn.de

ABSTRACT: If SUSY is discovered at the LHC, the task will immediately turn to determining the model of SUSY breaking. Here, we employ a Mixed Modulus-Anomaly Mediated SUSY Breaking (MMAMSB) model with very similar LHC phenomenology to the more conventionally studied Constrained Minimal SUSY Model (CMSSM) and minimal Anomaly Mediated SUSY Breaking (mAMSB) models. We then study whether the models can be distinguished and measured. If we only fit to the various mass edges and mass end-points from cascade decay chains that are normally studied, a unique determination and measurement of the model is problematic without substantial amounts of LHC data. However, if event rate information is included, we can quickly distinguish and measure the correct SUSY model and exclude alternatives.

Contents

1	Introduction	1
2	Mixed moduli-anomaly mediated supersymmetry breaking	4
3	MMAMSB model point	5
4	Fit procedure	6
4.1	Kinematic edges	9
4.2	Rates	10
5	Fit results	11
5.1	MMAMSB	11
5.2	CMSSM	17
5.3	mAMSB	21
6	Discussion	23

1 Introduction

The experiments at the Large Hadron Collider (LHC) are currently running and have begun to explore physics at the Terascale. In particular, the LHC has already probed large regions of the parameter space of supersymmetry (SUSY), one of the most well motivated and thoroughly studied approaches to solving the hierarchy problem [1–13].

Generically, the dominant signature for R-parity-conserving SUSY at the LHC is events with high transverse momentum (p_T) jets (and maybe leptons) accompanied by large amounts of missing transverse energy (E_T^{miss}), originating from the pair production of squarks and gluinos which then cascade decay eventually to the lightest neutralino (LSP). Indeed, the strongest limits to date on the supersymmetric parameter space come from searches for events with multiple hard jets plus missing energy and zero or one lepton [5, 7, 12, 13].

If new physics consistent with SUSY is discovered at the LHC, these cascade decay events may also be instrumental in determining the Lagrangian parameters of the underlying model. Various kinematic edges can be constructed from the jets, leptons, and missing energy. The measurement of these edges then constrains the SUSY mass spectrum [14–17]. Combined with additional measurements of sparticle decay branching ratios, these measurements can be used as input into a global fit for the parameters of a given SUSY model.

Several groups have performed such fits for various supersymmetric parameter spaces [18–23]. In a sufficiently low-dimensional parameter space such as the constrained minimal supersymmetric standard model (CMSSM) and with sufficient luminosity, the LHC measurements are powerful enough to enable a precise determination of the best-fit SUSY parameters. With low luminosity and/or in a parameter space with a greater number of degrees of freedom, however, the endpoint and branching ratio measurements alone are not always sufficient to ensure a stable fit and a precise parameter determination.

In Ref. [18], it was demonstrated that the inclusion of a cross section measurement—in particular the rate of high-missing- p_T events—can drastically improve the precision of a fit to a SUSY parameter space with non-universal gaugino masses. The authors of Ref. [18] use a standard leading-order Monte Carlo simulation and a fast detector simulation to compute the rate at each point in parameter space. While this method is straightforward and general, there are some technical challenges to this approach that have so far made it impractical to include rates in most such fits.

The first issue is the computational cost of a Monte Carlo simulation. In Ref. [18], this is addressed by only generating a small number (1000) of events per parameter space point, and by implementing a parallelized version of the Monte Carlo generator `Herwig` [24] on multiple processors. Even so, the computation of rates is extremely time-consuming and it is only feasible to scan a relatively small number of parameter space points when doing the fit. Because of the limitation on the number of events that can be generated per point in parameter space, there are also large statistical fluctuations in the computed rate. These fluctuations can spoil the stability of the fit. Finally, while the state-of-the-art calculations of SUSY production cross sections at the LHC include many higher-order corrections, the Monte Carlo generators only use leading-order cross sections.

Recently, a technique to include rate information in fits and overcome the issues listed above was presented in Ref. [25], and was implemented in the fitting code `Fittino` [26]. In this implementation, the cross section for sparticle production is first interpolated from a grid in the space of sparticle masses that was pre-computed using the program `Prospino` [27]. The remaining factor in the event rate, the acceptance—the fraction of sparticle production events whose decay products pass the kinematical cuts—is computed using a novel semi-analytical method. Because computing the rate in this way is extremely fast and sufficiently accurate, it allows event rates to be used on the same footing as the usual edge measurements in fits to LHC data. We use this technique as implemented in `Fittino` in the fits performed here and find that the rates are often a crucial ingredient in obtaining convergent and precise measurements of SUSY parameters.

Of course, we do not a priori know the mechanism of supersymmetry breaking, and thus which SUSY parameter space is the appropriate one in which to run such a fit. Most fits have concentrated on the CMSSM parameter space, because it involves a small number of parameters and because it has been extremely well studied. One could of course ask, would LHC measurements provide sufficient information to select one model of SUSY breaking over another? In other words, would a fit performed in the “wrong” parameter space yield a significantly worse goodness-of-fit than one performed in the “right” parameter space? This question was recently investigated [23] for a number of popular SUSY breaking models: the

CMSSM, which is a version of gravity-mediated SUSY breaking; minimal gauge-mediated SUSY breaking (mGMSB); minimal anomaly mediation (mAMSB) and large-volume string compactification models. Assuming a signal with 1 fb^{-1} of LHC data at $\sqrt{s} = 14 \text{ TeV}$ it was found that the CMSSM scenario can be distinguished, using the LHC endpoint measurements only, from all other scenarios considered except for the mGMSB, which can fit the data considered equally well.

One SUSY breaking scenario that until now has not been studied in the context of a global fit is mirage mediation, also known as mixed modulus-anomaly mediated SUSY breaking (MMAMSB). This model is attractive theoretically because it can be derived from a concrete string compactification scenario due to Kachru, Kallosh, Linde and Trivedi (KKLT) which provides mechanisms for breaking SUSY, stabilizing unwanted moduli, and ensuring a positive cosmological constant [28]. In fact in Ref. [29] it is argued that the MMAMSB breaking pattern is a generic feature of a certain class of mechanisms that stabilize string moduli, of which the KKLT construction is only one example.

A couple of papers have analyzed the soft SUSY breaking terms that arise from specific realizations of this scenario, pointing out that the SUSY-breaking contributions from gravity (i.e. modulus) mediation are comparable to those coming from anomaly mediation [30, 31]. A parameter of the model, α , interpolates between pure anomaly mediation and pure modulus mediation. For vanishing α , the model suffers from the tachyonic slepton problem of pure AMSB, whereas for intermediate or large values of α , this problem is alleviated by the gravity-mediated contributions.

The phenomenology of MMAMSB has been studied in several papers [32–39], where it has been shown that there are good prospects for discovering this type of SUSY breaking scenario at the LHC and/or at direct dark matter detection experiments. At least for certain choices of the model parameters, it should also be possible to measure them and identify the gaugino mass pattern distinctive to this model.

In this paper, we aim to quantify the extent to which the MMAMSB scenario can be explored at the LHC by performing a global fit to prospective LHC measurements in the MMAMSB parameter space. This way, we can evaluate the accuracy and precision of the measurement of the model parameters. By attempting to fit different SUSY-breaking scenarios, the CMSSM and mAMSB, to the MMAMSB model, we can also evaluate whether LHC measurements are sufficient to distinguish MMAMSB from other SUSY-breaking scenarios. We show that the inclusion of rates as inputs to the fit is necessary to enable accurate parameter measurements with relatively low luminosity, and that rates are especially crucial in distinguishing MMAMSB from the CMSSM and mAMSB.

The layout of this paper is as follows. We begin by giving a brief introduction to the MMAMSB model and, in particular, the phenomenology of the gaugino sector. In Sec. 3, we discuss choosing a particular benchmark point in the model that satisfies all of the current experimental and observational constraints. In Sec. 4, we discuss how we fit the model with hypothetical LHC data and introduce the different observables that we use. Finally, in Sec. 5 we present the results of fitting the MMAMSB to observables derived from our benchmark point. We also try to fit other SUSY breaking models (the CMSSM and mAMSB) to our benchmark to see how quickly these models can be excluded and

which observables are effective at performing this task. We conclude with a discussion in Sec. 6.

2 Mixed moduli-anomaly mediated supersymmetry breaking

In this section we briefly introduce the MMAMSB scenario. We adopt the notation of Ref. [35]. As mentioned in the introduction, the MMAMSB can be derived from the KKLT string construction [28], or indeed from a class of string models in which moduli stabilization and SUSY breaking are accomplished dynamically [29]. In these models, the soft SUSY breaking terms receive contributions from both modulus and anomaly mediation. The parameter α interpolates between the pure modulus and pure anomaly extremes.

The soft terms also depend on the sets of parameters n_i and ℓ_a , which correspond to powers in the Kähler potential for matter fields and the gauge kinetic functions respectively. In the KKLT construction, ℓ_a can take on the value 0 or 1 depending on whether the corresponding gauge field is localized on a $D3$ or $D7$ brane, whereas n_i can be 0, 1, or $1/2$ for a matter field localized on a $D7$ brane, a $D3$ brane, or a brane intersection.

Here we concentrate on the scenario where $\ell_a = 1$ for all gauge fields and where $n_i = n$ for all matter fields (including the Higgs fields). Having a common value for n_i among the sfermions is motivated by flavor constraints. Having a different n_i for the sfermions and the Higgses is possible, but for simplicity we assume a common value here. With these assumptions, the soft SUSY breaking parameters—the gaugino mass parameters, trilinear couplings, and sfermion mass parameters, respectively—at the GUT scale are given by

$$M_a = \frac{m_{3/2}}{16\pi^2} [\alpha + b_a g_a^2], \quad (2.1)$$

$$A_{ijk} = \frac{m_{3/2}}{16\pi^2} [3(n-1)\alpha + (\gamma_i + \gamma_j + \gamma_k)], \quad (2.2)$$

$$m_i^2 = \left(\frac{m_{3/2}}{16\pi^2} \right)^2 [(1-n)\alpha^2 + 4\alpha\xi_i - \dot{\gamma}_i]. \quad (2.3)$$

Here, $m_{3/2}$ is the gravitino mass, g_a is the gauge coupling and $b_a = (\frac{33}{5}, 1, -3)$ the 1-loop β function coefficient for the gauge group a . The anomalous dimensions γ_i and their logarithmic derivatives $\dot{\gamma}_i$ as well as the mixed anomaly-modulus contributions ξ_i are given in Appendix A of Ref. [33].

In Eq. (2.1) the term proportional to α is the universal gravity mediation contribution, whereas the second term is the anomaly mediation contribution. The ratio of gauge couplings at the TeV scale should be a combination of the expected ratio from gravity mediation,

$$M_1 : M_2 : M_3 \simeq 1 : 2 : 6, \quad (2.4)$$

and the expected ratio from anomaly mediation,

$$M_1 : M_2 : M_3 \simeq 3.3 : 1 : 9. \quad (2.5)$$

For the MMAMSB, it is¹

$$M_1 : M_2 : M_3 \simeq (\alpha + 3.3) : (2\alpha + 1) : (6\alpha - 9). \quad (2.6)$$

This distinct ratio of couplings is a hallmark sign of this model, and suggests that measuring the weak-scale gaugino masses could enable one to determine α .

In pure anomaly mediation, there is a well-known problem of tachyonic slepton masses, which in the standard mAMSB scenario is solved by adding an ad hoc common term to all the sfermion masses. In this model, for moderate values of α the tachyonic slepton problem is solved by the gravity mediation contributions, and this term does not need to be included.

3 MMAMSB model point

In order to carry out a fit in the MMAMSB parameter space, we first need to select a point in this space to serve as our model. For a given point in parameter space, then, we must compute the spectrum and check that various constraints are satisfied and desirable features are present.

We use the ISASUGRA spectrum generator that is packaged with ISAJET [40] to compute the RGE running of the parameters and to compute the low-energy spectrum and decays. We then use a number of codes to check various constraints: the IsaTools package provided with ISAJET and the programs SuperIso Relic [41] and micrOMEGAs [42–44]. Each of these codes computes the relic density and various precision low energy and flavor constraints, and IsaTools and micrOMEGAs also compute dark matter direct detection cross sections. We also check that the model has not been ruled out by Higgs searches using HiggsBounds [45].

We consider scenarios with $1 \lesssim \alpha \lesssim 10$, that have roughly similar SUSY breaking contributions from each sector and are close to the original KKLT construction value of $\alpha = 5$.

In order for a fit using standard LHC observables, especially the kinematic endpoints, to be feasible, the decay chain

$$\tilde{q} \rightarrow q\tilde{\chi}_2^0 \rightarrow q\ell^\pm\tilde{\ell}_R^\pm \rightarrow \ell^+\ell^-\tilde{\chi}_1^0 \quad (3.1)$$

must be present with a sufficiently large branching ratio. This means that the $\tilde{q} \rightarrow \tilde{\chi}_2^0$ and $\tilde{\chi}_2^0 \rightarrow \tilde{\ell}_R$ decays must have sizeable branching ratios and sufficiently large mass splittings to give rise to hard enough jets and leptons to pass experimental cuts. In addition, the squark masses must be sufficiently low to give reasonable squark production cross sections at the LHC, but not so low that they are clearly ruled out by early LHC searches.

¹In this paper we follow the notation of Ref. [35] by Baer et al., in particular $\alpha = \alpha_{\text{Baer}}$. As pointed out in that reference, however, the reader should be warned that elsewhere in the literature, e.g. Refs. [29, 32] by Choi et al., α is defined such that $\alpha_{\text{Choi}} = \frac{16\pi^2}{\log(M_P/m_{3/2})} \frac{1}{\alpha_{\text{Baer}}}$. The coupling ratio as a function of α will of course be a different function of α_{Choi} .

Parameter	Value	Parameter	Value
α	4.8	M_1	460.6
$m_{3/2}$	21×10^3	M_2	556.0
$\tan \beta$	10	M_3	976.7
$\text{sign}(\mu)$	+1		
n	0.5		

Table 1. MMAMSB benchmark point. All masses in GeV.

For simplicity, we choose a common value of the modular weights n_i for all of the sfermion and Higgs fields. In order to satisfy the branching ratio and mass splitting requirements just mentioned, we find that in this case $n = 1/2$ is the only valid choice. There is some freedom in choosing $\tan \beta$ and $\text{sign}(\mu)$, so we adopt the SPS1a [46] values $\tan \beta = 10$ and $\text{sign}(\mu) = +1$.

Performing a scan over the remaining parameters α and $m_{3/2}$, we find that the strongest constraint on finding a viable model is the measurement by the WMAP experiment [47] of the dark matter relic density. The computed relic density takes on a value within the observed error bars in only narrow strips of the $\alpha - m_{3/2}$ plane². One such region is an almost-vertical strip at $\alpha \simeq 4.8$, with $m_{3/2}$ ranging from 15 TeV upwards, where a mostly bino though somewhat mixed $\tilde{\chi}_1^0$ undergoes efficient annihilation into $h A$, $b \bar{b}$, $W^+ W^-$ and $Z H$. From this region we select the benchmark point with $m_{3/2} = 21$ TeV. The model parameters and the weak-scale gaugino mass parameters are summarized in Tab. 1.

This model satisfies all the observational constraints implemented in the codes mentioned above, though the spin-independent direct detection cross section is right on the edge of the XENON100 [48] limit. The value of α is close to the value preferred by the KKLT string scenario ($\alpha_{\text{KKLT}} = 5$), and is far enough from the gravity-mediated and anomaly-mediated limits to give distinct phenomenology. In particular, the gaugino mass ratio (at the weak scale) in this model is $M_1 : M_2 : M_3 \simeq 1 : 1.2 : 2.2$, which is quite distinct from the ratio $1 : 2 : 6$ expected from gravity mediation, and $3.3 : 1 : 9$ expected from anomaly mediation. The model also has the branching ratios and mass differences mentioned above that are required for the standard LHC observables.

The full spectrum of the model is given Tab. 2, and is plotted in Fig. 1 alongside the SPS1a spectrum for comparison. Benchmark planes and lines for further LHC studies of MMAMSB models have been proposed in Ref. [49]

4 Fit procedure

In order to perform the fits we use the `Fittino` program [26]. `Fittino` first requires an input file, in which the user specifies the set of observables and provides their (perhaps

² For a given parameter point, the calculated relic density can vary significantly depending on which code is used to compute it and on which spectrum calculator is used. Because the relic density depends on the spectrum, and thus the model parameters, this difference can be undone by a slight change in the parameters and thus does not affect our results.

Particle	Mass	Particle	Mass	Particle	Mass
\tilde{d}_L	939.3	$\tilde{\ell}_L$	535.9	$\tilde{\chi}_1^0$	439.8
\tilde{d}_R	907.5	$\tilde{\ell}_R$	478.5	$\tilde{\chi}_2^0$	498.8
\tilde{u}_L	935.7	$\tilde{\tau}_1$	469.4	$\tilde{\chi}_3^0$	529.2
\tilde{u}_R	908.3	$\tilde{\tau}_2$	533.8	$\tilde{\chi}_4^0$	611.7
\tilde{b}_1	837.6			$\tilde{\chi}_1^\pm$	487.6
\tilde{b}_2	899.0			$\tilde{\chi}_2^\pm$	608.7
\tilde{t}_1	613.2			\tilde{g}	1021.8
\tilde{t}_2	894.2				

Table 2. MMAMSB benchmark model. All masses in GeV.

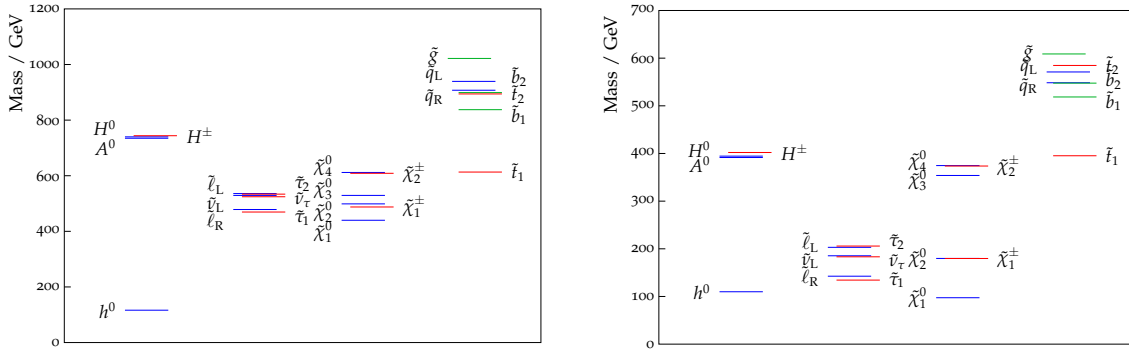


Figure 1. The spectrum of our MMAMSB model (on the left) compared to the spectrum of SPS1a (on the right). Note the difference in scales on the vertical axis.

hypothetical) measured values and uncertainties. Here the user also specifies the supersymmetric model and the high or low scale parameters to be fitted along with their starting values. `Fittino` then efficiently samples the parameter space, finds the best fit point and maps out confidence regions (*i.e.*, contours of the likelihood function) using Markov chain Monte Carlo.

It is important to emphasize that in the fits we perform here, we only use LHC observables as inputs. While it is possible with `Fittino` to also include in the fits the various low-energy, flavor, and astrophysical observables that were used in the previous section to pick a benchmark model, we focus instead on the power of the LHC alone to constrain and measure the model parameters.

In order to compute the likelihood function at each point in parameter space visited by the Markov chain, `Fittino` first calls an external code to calculate the mass spectrum, decay widths, and branching ratios. We use the `ISASUGRA` spectrum calculator, since it includes the MMAMSB scenario.

The predicted values of the chosen observables are then computed internally by `Fittino` or by an external code, and compared with the measured values to compute the likelihood. Originally, `Fittino` included among its LHC observables a large set of kinematical edges, as well as some branching ratio observables. Crucial to our analysis will be the inclusion

of event rates, which, as mentioned earlier, were implemented as observables in `Fittino` in Ref. [25].

In this implementation, `Fittino` first uses the decay table computed by the spectrum calculator to determine the branching ratios of the squark- and gluino-initiated decay chains that could contribute to the given channel. Each branching ratio is then multiplied by the relevant squark and/or gluino production cross section. This cross section is interpolated from a grid over $m_{\tilde{q}}$ and $m_{\tilde{g}}$ of NLO cross sections that have been previously computed using the code `Prospino` [27, 50, 51]. It remains to compute the acceptance, i.e. the fraction of events which pass the analysis cuts for the given channel. As is described in detail in Ref. [25], in this implementation the acceptance is computed by combining analytical formulae for the momentum distributions of the decay products of at-rest squarks and gluinos with numerical estimates (which are also interpolated from pre-computed grids) of the effect of boosting the system into the lab frame.

It was shown in Ref. [25] that this fast technique for estimating the acceptance agrees to within 5% with acceptances determined using Monte Carlo event generation. To verify that this agreement holds within the parameter space of the MMAMSB scenario, we computed acceptances across a grid in MMAMSB parameter space using `Herwig++` [52, 53] to generate events and `Rivet` [54], including the anti- k_t jet finder [55, 56], to apply the cuts. We then performed some of our MMAMSB fits using acceptances interpolated from these grids alongside the fits using the rates code implemented in `Fittino`, and found very good agreement.

An extremely important ingredient in the calculation of the likelihood is the estimate of the uncertainty on each observable. For the well-studied SPS1a model, which is the basis of the `Fittino` fits performed in Refs. [19, 25], the uncertainties for most observables can be obtained from the thorough study carried out in Ref. [17]. For the fit we perform here, we must extrapolate these uncertainties from SPS1a to our MMAMSB model. To do this, we must take into account the relative number of events from SPS1a and our model in each signal channel. In our MMAMSB model, the squarks and gluino have higher masses than they do in SPS1a, so the production cross sections are lower, leading to fewer signal events and thus larger uncertainties on most observables. In some cases, however, an increase in branching ratios between models can more than make up for the decrease in cross section. For example, the branching ratio of the decay $\tilde{\chi}_4^0 \rightarrow \tilde{\ell}_R^\pm \ell^\mp$ is ten times larger in our model than in SPS1a, leading to a much more pronounced di-lepton edge due to $\tilde{\chi}_4^0$ decays.

To verify that the scaling of uncertainties we performed is reasonable, we looked at one of the observables, the $m_{\ell\ell}$ endpoint (for a more detailed description of each observable, see the next two subsections) in detail. We generated events for SPS1a and our MMAMSB model, including energy smearing to account for detector effects. We then fit a smeared step function to the data in order to extract the endpoint and determine its uncertainty. The uncertainties we obtained in this way roughly match the SPS1a uncertainties given in Ref. [17] and the uncertainties we extrapolated from this for our MMAMSB model, verifying the reasonableness of our extrapolations. For illustration, in Fig. 2 we show the $m_{\ell\ell}$ distribution, with statistical error bars, for each model for a particular choice of center-of-mass energy and integrated luminosity, with the fitted function superimposed over the

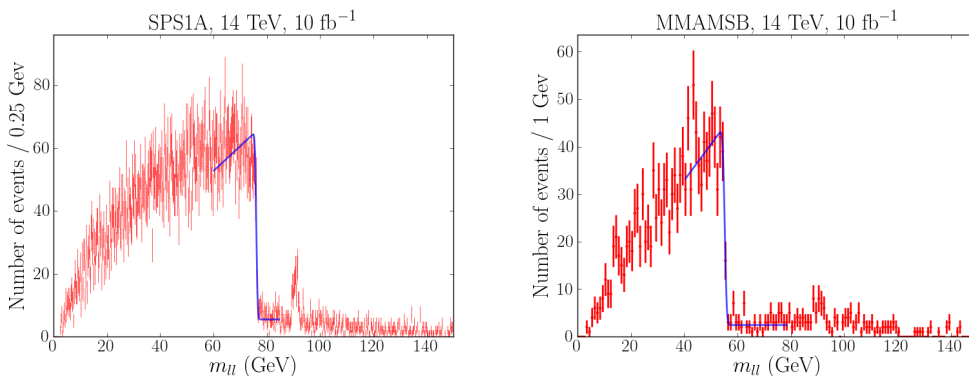


Figure 2. The $m_{\ell\ell}$ distribution for SPS1a (left) and the MMAMSB model (right) for 10 fb^{-1} of integrated luminosity at the LHC with $\sqrt{s} = 14 \text{ TeV}$. The error bars show the statistical error only. Superimposed is the fit function used to extract the endpoint value.

data.

4.1 Kinematic edges

Throughout this paper, we compare the impact of various sets of observables on the fits. The first two sets below do not include rates, and are mostly edges of kinematical distributions. The basic set we call Group I and includes standard kinematical edges built from the “golden” decay chain described earlier. Group II contains additional quantities built from this decay chain as well as some observables sensitive to the properties of third generation sparticles. The full list of Group I and II observables is as follows:

- List of observables in Group I (these are all defined in Ref. [16]).
 - $m_{\ell\ell}^{\text{max}}$, the dilepton invariant mass edge.
 - $m_{q\ell\ell}^{\text{max}}$, the jet dilepton invariant mass edge.
 - $m_{q\ell}^{\text{low}}$, the jet-lepton low invariant mass edge.
 - $m_{q\ell}^{\text{high}}$, the jet-lepton high invariant mass edge.
- List of observables in Group II.
 - $m_{q\ell\ell}^{\text{thr}}$, the jet-dilepton threshold invariant mass edge [16].
 - $m_{\tilde{q}}^{T2}$, the squark transverse mass [57, 58].
 - $m_{\tau\tau}^{\text{max}}$, the di-tau invariant mass edge [17, 19].
 - m_{tb}^w , the weighted top-bottom invariant mass edge [19].
 - $\Delta m_{\tilde{g}\tilde{\chi}_1^0}$, the mass difference between the gluino and the LSP [17, 19].
 - $m_{(\tilde{\chi}_4^0)\ell\ell}^{\text{max}}$, the dilepton invariant mass edge from the decay of a $\tilde{\chi}_4^0$ [17, 19].
 - $r_{\tilde{\ell}\tilde{\tau}}^{\text{BR}}$, the ratio of selectron (smuon) to stau mediated $\tilde{\chi}_2^0$ decays [19].

Observable	Nominal value	Uncertainty					
		10 fb ⁻¹ 7 TeV	1 fb ⁻¹ 14 TeV	10 fb ⁻¹ 14 TeV	100 fb ⁻¹ 14 TeV	LES	JES
Group I							
$m_{\ell\ell}^{\max}$	55.45	6.01	4.25	1.34	0.43	0.05	-
$m_{q\ell\ell}^{\max}$	373.4	70.2	49.6	15.7	4.96	-	3.7
$m_{q\ell}^{\text{low}}$	223.3	38.0	26.8	8.5	4.40	-	2.2
$m_{q\ell}^{\text{high}}$	311.9	26.0	18.4	5.8	4.70	-	3.1
Group II							
$m_{q\ell\ell}^{\text{thr}}$	145.5	-	-	29.6	9.37	-	1.5
$m_{\tilde{q}}^{T^2}$	662.0	-	-	28.2	8.91	-	7.0
$m_{\tau\tau}^{\max}$	58.94	-	-	15.9	5.04	-	0.6
m_{tb}^w	494.1	-	-	43.0	13.6	-	4.9
$\Delta m_{\tilde{g}\tilde{\chi}_1^0}$	582.0	-	-	48.5	15.3	-	5.8
$m_{(\tilde{\chi}_4^0)\ell\ell}^{\max}$	168.6	-	-	9.96	3.15	0.17	-
$r_{\ell\tilde{\tau}}^{\text{BR}}$	0.457	-	-	0.0114	0.0036	-	-

Table 3. LHC observables for the MMAMSB benchmark point, Tab. 1. The masses and branching ratios have been calculated with ISASUGRA [40]. The uncertainty estimates on the observables are based on [17, 19] and have been rescaled as described in the main text. All dimensionful quantities are given in GeV.

In Tab. 3 we provide, for each observable, its nominal value in our MMAMSB model and its uncertainty, determined by scaling from SPS1a as described above, for each luminosity and center-of-mass energy scenario. The last two columns give additional contributions to the uncertainty from the lepton energy scale and jet energy scale [19].

4.2 Rates

In addition to the Group I and II observables listed in the previous subsection, we also consider the two rate observables discussed previously. Here, we give the description of these observables, including the full list of cuts.

- List of rate observables. (These observables are also defined in Ref. [25].)
 - $R_{jj\cancel{E}_T}$, the event rate for at least two hard jets and missing transverse energy.
 - * $p_{T,\text{jet}} > 50$ GeV.
 - * $|\eta_{\text{jet}}| < 2.5$.
 - * $R_{\text{jet}} = 0.4$ (anti- k_t jet algorithm [55, 56]).
 - * $\cancel{E}_T > 100$ GeV.
 - $R_{\ell\ell jj\cancel{E}_T}$, the event rate for at least two hard jets and missing transverse energy with a pair of opposite sign, same flavour leptons (1st or 2nd generation). The

Observable	7 TeV		14 TeV	
	Value (fb)	Uncertainty	Value (fb)	Uncertainty
$R_{jj\cancel{E}_T}$	113	23	2780	556
$R_{\ell\ell jj\cancel{E}_T}$	11.8	3.5	245	49

Table 4. LHC event rates for the MMAMSB benchmark point, Tab. 1. The event rate includes the NLO squark and gluino production cross section [50, 51], the branching ratios of the decays and the expected particle acceptances. The acceptances were tested with full parton shower and hadronisation using Herwig++ [52, 53], Rivet [54] and the anti- k_t jet finder [55, 56].

background from the leptonic decays of τ leptons, $\tilde{\chi}_{1,2}^\pm$ and W^\pm is removed by subtracting events with opposite sign, different flavour lepton pairs.

- * $R_{jj\cancel{E}_T}$ signal.
- * $p_{T,\ell} > 10\text{GeV}$.
- * $|\eta_\ell| < 2.5$.
- * Lepton-jet isolation of $\Delta R = 0.2$ (jet activity within $\Delta R = 0.2 < 10$ GeV).

In Tab. 4, we provide the values for these observables, *i.e.* the event rates for the two different types of events as predicted by a Monte Carlo simulation. We provide the rates and their uncertainties for both 7 and 14 TeV.

5 Fit results

In this section we present the main results of our paper and show that including event rates in fits can significantly increase their effectiveness to measure and exclude different SUSY breaking scenarios. We begin by fitting to our own MMAMSB benchmark scenario and show that even with early data, the model can be constrained and some parameters measured accurately. With larger data sets, we should be able to measure the whole of the parameter space with high accuracy ($\lesssim 5\%$).

We then try to fit other SUSY breaking scenarios to our benchmark point from MMAMSB. We start with the CMSSM and show that if we only include the Group I mass edges, a good fit can be achieved unless we have very large data sets (100fb^{-1} at 14 TeV). However, if we include event rates in the fit, we see that even with a small amount of data (10fb^{-1} at 7 TeV), we can exclude the CMSSM. We complete the same task for the mAMSB and see very similar results. With Group I observables and early data we cannot conclusively exclude the scenario. However, as soon as we add event rates, the model can no longer fit the data.

5.1 MMAMSB

In this section we discuss the results of fitting the MMAMSB model to observables derived from our benchmark scenario. Fits are performed for 10fb^{-1} at 7 TeV and 1fb^{-1} , 10fb^{-1} , and 100fb^{-1} at 14 TeV. In addition, we also show the effect of adding rates (see Tab. 4)

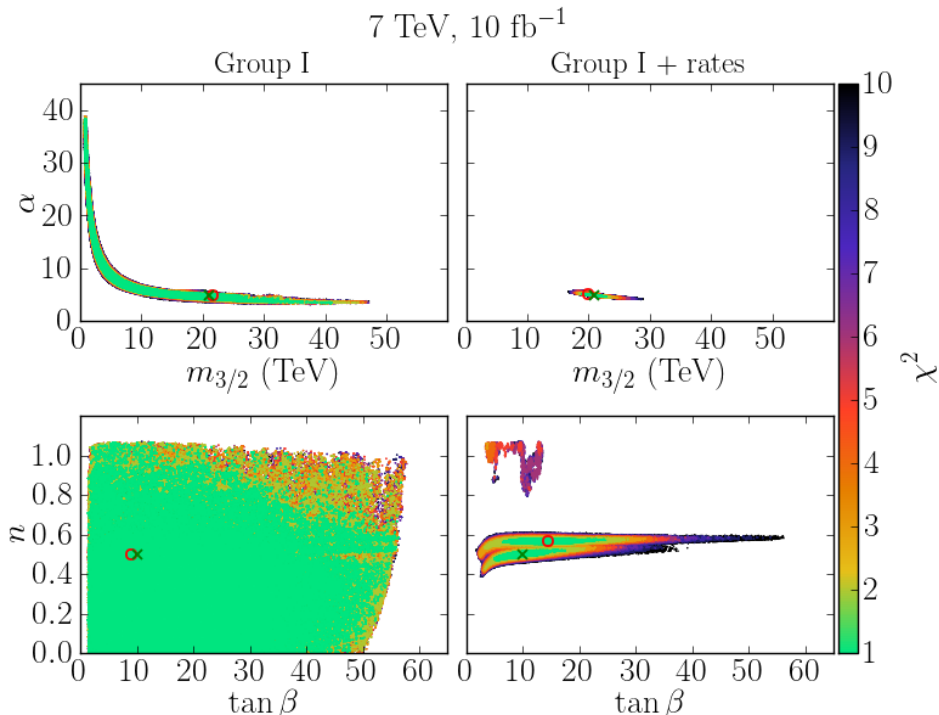


Figure 3. $1\text{-}\sigma$ (68.3%) (black), $2\text{-}\sigma$ (95.4%) (grey), and $3\text{-}\sigma$ (99.7%) (light grey) two-dimensional confidence regions for 7 TeV, 10 fb^{-1} , using Group I observables, without (left column) and with (right column) rates. The green ‘X’ represents the input point and the red circle the best-fit point.

to the fits, and including the more complicated set of Group II observables (see Tab. 3). We demonstrate that rates significantly improve the accuracy of the fits, especially when using early LHC data with limited statistics.

Let us first consider the fits that can be performed with 10 fb^{-1} at 7 TeV and 1 fb^{-1} at 14 TeV. With this amount of data and our benchmark scenario, we do not expect to have sufficient statistics to be able to measure any of the observables given in Group II. Therefore, we perform the fits using the mass edges in Group I, both with and without the rates. In the left-hand column of Figs. 3 and 4, we see that when only using the Group I edges, the model is essentially unconstrained across the whole parameter space and an effective fit cannot be performed.

As soon as we add rates to the fit, however, the situation improves remarkably. At our benchmark point we can now constrain $m_{3/2}$ to $\sim 15\%$ and α to $\sim 10\%$ as can be seen in the right-hand column of Figs. 3 and 4, or in the zoomed-in version of these regions shown in Fig. 5. The fact that the rates improve the constraints on $m_{3/2}$ and α is to be expected if we examine the form of the soft breaking terms in the MMAMSB model, Eqs. (2.1)-(2.3). We see that the soft breaking masses are all proportional to the product $\alpha m_{3/2}$. Therefore, the rate observables, which are sensitive to the overall mass scale of any new states, constrain this combination effectively. The modular weight, n , is less well constrained—at 7 TeV it is only determined within $\sim 20\%$, as can be seen in Fig. 5—due

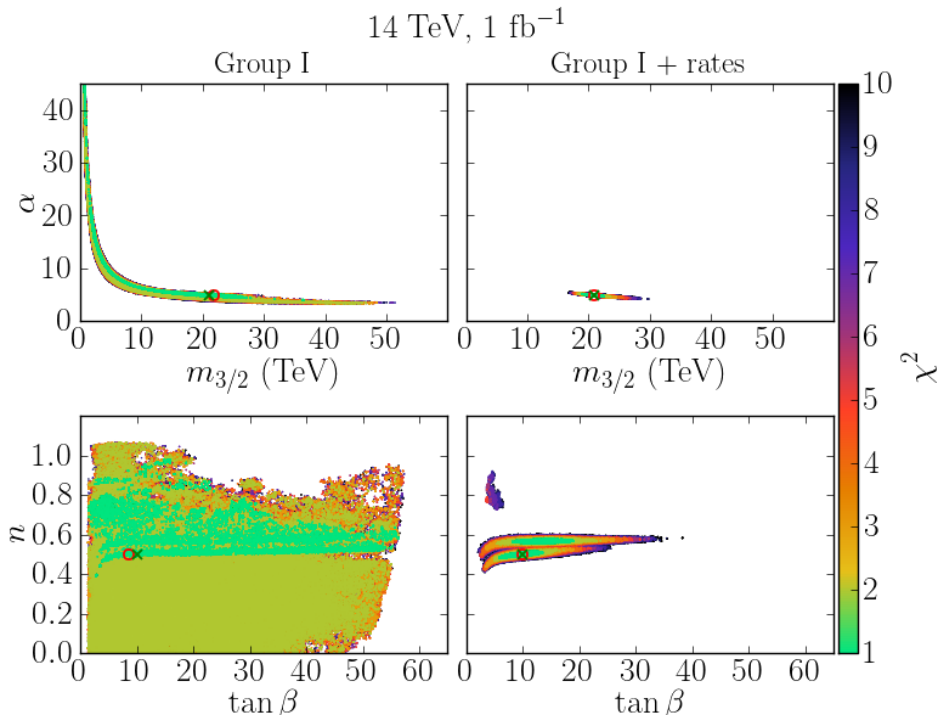


Figure 4. Like Figure 3 except for 14 TeV, 1 fb⁻¹.

to the fact that it has a sub-leading dependence in the soft breaking terms. This is still an improvement, however, over the fit without rates, where n could not be constrained at all. Finally, $\tan\beta$ has the worst constraints of all the parameters in the fit; even with rates included, most values are allowed. As we show later, a measurement of $\tan\beta$ requires observables that are sensitive to third-generation particles and none of the observables in Group I measure these.

If we move to the fits with 10 fb⁻¹ at 14 TeV, we see in Fig. 6 that even an accurate determination of all the Group I mass edges can still not constrain the MMAMSB model in any parameter. Once we add the information from rates, we again see a good fit for $m_{3/2}$, α and n , and even $\tan\beta$ is constrained ($\tan\beta = 10^{+8.5}_{-3.5}$). The reason that $\tan\beta$ can be constrained with the rate observables is that the combination of $R_{jj\cancel{\Psi}_T}$ and $R_{\ell\ell jj\cancel{\Psi}_T}$ acts as an observable for the branching ratio of the decay $\tilde{\chi}_2^0 \rightarrow \tilde{\ell}^\pm \ell^\mp$. This branching ratio is sensitive to $\tan\beta$ since it competes with the branching ratio of the decay $\tilde{\chi}_2^0 \rightarrow \tilde{\tau}^\pm \tau^\mp$, which increases substantially as $\tan\beta$ becomes large.

Adding the Group II set of observables with a reasonable statistical error becomes possible with 10 fb⁻¹ at 14 TeV. We can now compare the fit using the Group I and II observables alone with that of using just the Group I observables along with rates. We see in Fig. 7 that in general the fit is greatly improved, especially for $\tan\beta$ and n . The constraining power for $\tan\beta$ mainly comes from the ratio $r_{\tilde{\ell}\tilde{\tau}}^{\text{BR}}$ and the mass edge $m_{\tau\tau}$. These observables directly measure the contribution of third generation superpartners, which is most sensitive to $\tan\beta$. The measurement of the mass scale $m_{3/2}$ is not improved

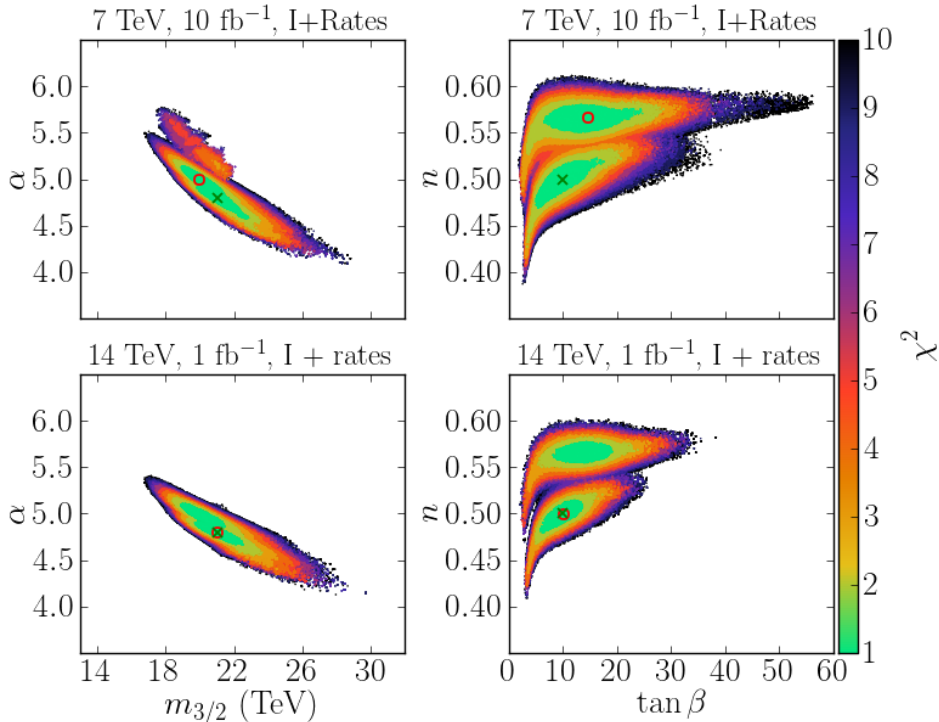


Figure 5. A zoomed-in view of the confidence regions for 7 TeV, 10 fb^{-1} and 14 TeV, 1 fb^{-1} . These are the same fits as in Fig. 3 and Fig. 4.

significantly, however, as this was already well constrained by the rate information. In the Group II observables, the squark transverse mass (m_q^{T2}) and the jet-dilepton threshold (m_{ql}^{thr}) now perform this task.

Despite the extra observables that constrain the mass scale in Group II, if we add rates to the fit, the measurement of both $m_{3/2}$ and α improves substantially, as is clear from Fig. 7. As stated before, this is due to the rates being particularly sensitive to the overall mass scale. The measurement of $m_{3/2}$ is improved by almost a factor of 2.

An interesting feature of the fits that now becomes much more clear is the double minimum seen in the $\tan \beta - n$ plane. The double minimum is due to the fact that the functional forms for m_{ql}^{\max} , m_{ql}^{low} and m_{ql}^{high} depend on the relative mass ratios of the particles in the cascade decay [15, 16]. For example, in the correct minimum we have a mass ordering $2m_\ell^2 > m_{\tilde{\chi}_1^0}^2 + m_{\tilde{\chi}_2^0}^2 > 2m_{\tilde{\chi}_1^0} m_{\tilde{\chi}_2^0}$, which leads to the end-points given in Tab. 3. However, in the second minimum, the mass ordering switches to $m_{\tilde{\chi}_1^0}^2 + m_{\tilde{\chi}_2^0}^2 > 2m_{\tilde{\chi}_1^0} m_{\tilde{\chi}_2^0} > 2m_\ell^2$, where the end-points have a different functional form. Thus, a different set of masses can lead to the same end-points being measured at the LHC. The problem of end-point mimics was previously been discussed in Refs. [59, 60] and possible solutions proposed were to measure the $\tilde{\chi}_1^0$ mass accurately at a linear collider [61, 62] or to measure the whole invariant mass distribution as the shape would be different for the mimic distribution. Unfortunately, the rates are unable to resolve the end-point mimics as they are only weakly sensitive to the masses of the electroweak particles further down the decay chain. The rates

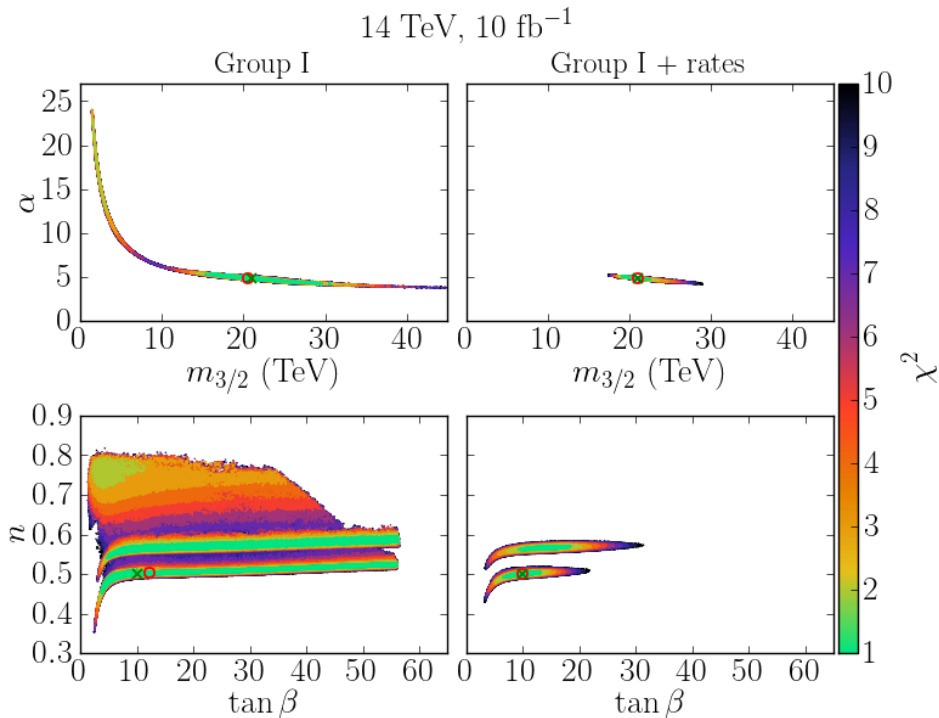


Figure 6. Confidence regions for 14 TeV, 10 fb⁻¹, only including Group I observables, with (left column) and without (right column) rates.

are most sensitive to the first generation squarks and gluino masses and in both minima, these are very similar.

With 100 fb⁻¹ of data, the Group I mass edges are all measured with high accuracy. Consequently, these mass edges alone can constrain all of the parameters apart from $\tan\beta$ to some extent, as can be seen in Fig. 8. Adding the rates to the fit, though, improves the measurements significantly. We see a large improvement in the determination of $m_{3/2}$ (the width of the 1 σ confidence region drops from 10 TeV to 4 TeV) and α , while $\tan\beta$ is becoming constrained.

If we include Group II observables to the above fits, as shown in Fig. 9, we now achieve a precision determination of better than 5% on all parameters. In fact, α , which parameterises the ratio of gauge couplings [see Eq. (2.6)] is measured to better than 1%. In addition, the double minimum displayed in other fits is no longer present and we now have no mass ordering ambiguity. The observable that breaks the ambiguity is $m_{\tau\tau}^{\max} = 32.0$ GeV (measured 58.9 GeV) which is 5.3 σ away. This is tensioned against $m_{\ell\ell}^{\max}$ which is the most accurately measured observable. If we want to increase $m_{\tau\tau}^{\max}$ for this point, we would also increase $m_{\ell\ell}^{\max}$, leading to an even worse fit.

In the high accuracy fits using 100 fb⁻¹ (Figs. 8 and 9), two interesting correlations become apparent. First, in the $m_{3/2}$ - α plane, there is a negative correlation between the two parameters. This correlation can be easily understood when we inspect the form of the soft breaking terms in the model, Eqs. (2.1)-(2.3). All of the soft masses are $\propto \alpha m_{3/2}$.

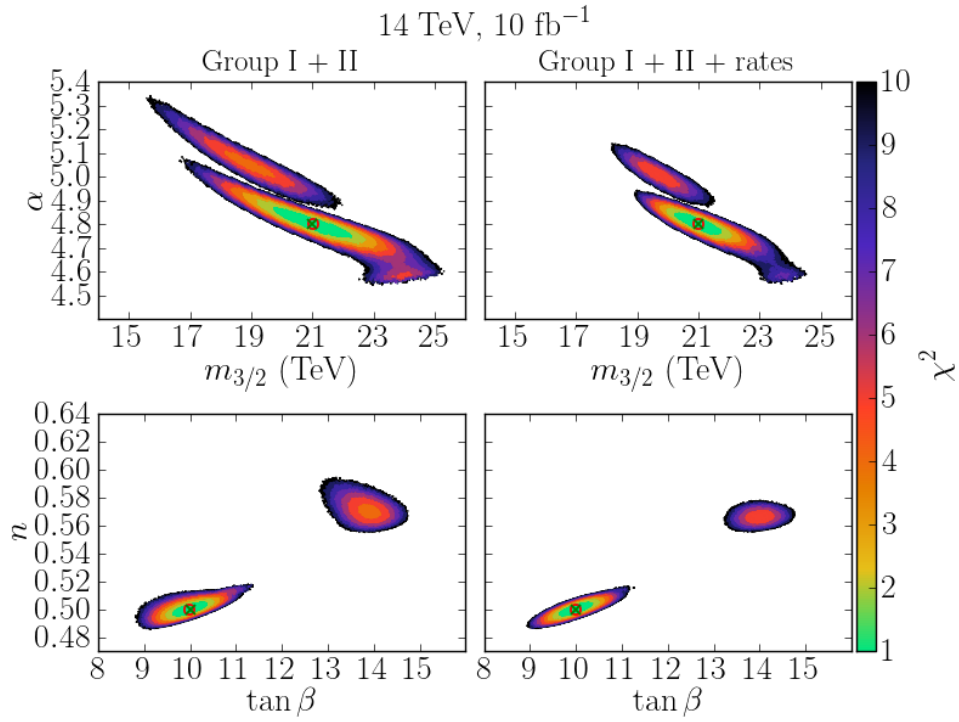


Figure 7. Like Fig. 6, but now also including Group II observables.

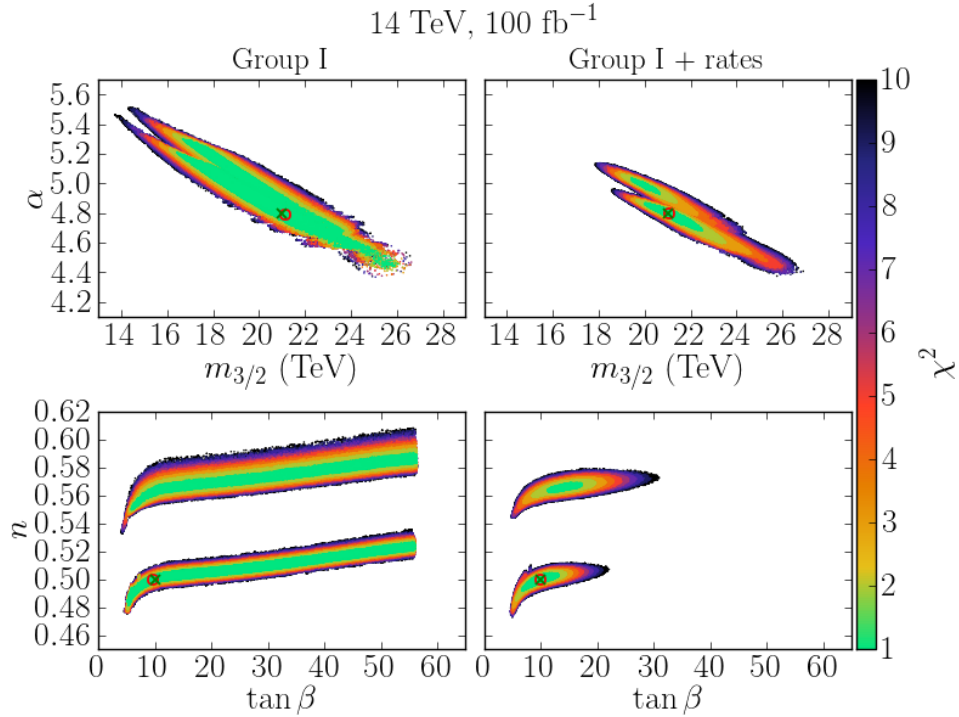


Figure 8. Like Fig. 6, but using 100 fb^{-1} .

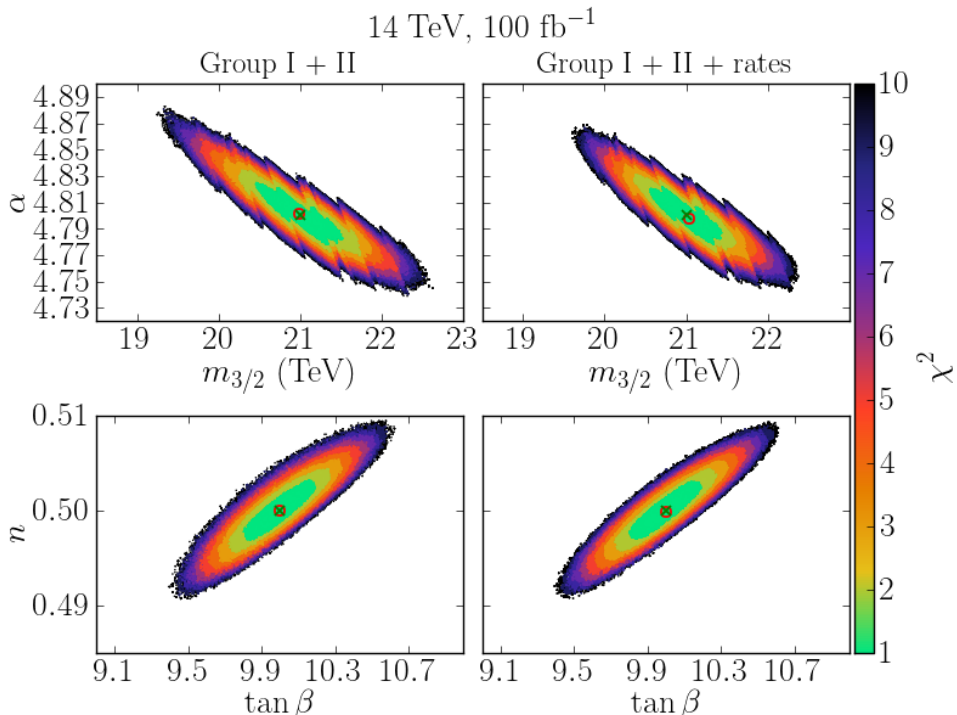


Figure 9. Like Fig. 7, but using 100 fb⁻¹.

Therefore to keep the particle masses at a set value, as $m_{3/2}$ increases, α must decrease and vice versa.

The other clear correlation is a positive one between the parameters $\tan \beta$ and n . This correlation is due to the trilinear coupling A_{ijk} which enters in the $\tilde{\tau}$ mixing matrix. The mixing term in the $\tilde{\tau}$ sector is

$$m_{\tilde{\tau}}^{mix} = m_{\tau}(A_{\tau} - \mu \tan \beta), \quad (5.1)$$

and from Eq. (2.2) we can see that $A_{\tau} \propto n$. Therefore, in order to keep the mixing in the $\tilde{\tau}$ sector constant, if n (A_{ijk}) increases $\tan \beta$ must also increase to compensate. The opposite would be true of the \tilde{t} sector but the observables $r_{\tilde{\ell}\tilde{\tau}}^{\text{BR}}$ and $m_{\tau\tau}^{\text{max}}$ are far more accurately measured than the observable m_{tb}^w . Thus the fit is dominated by the constraint in the $\tilde{\tau}$ sector.

The results of our MMAMSB fit are collected in Tab. 5.

5.2 CMSSM

In the previous section we have shown that we can accurately reconstruct our MMAMSB benchmark point at the LHC, even with relatively small amounts of data (10 fb⁻¹ at 14 TeV). Here we would like to determine, however, if it is also possible to rule out other SUSY breaking scenarios. Possibly the most widely studied scenario is the CMSSM and thus it is natural to ask what happens if we attempt to fit this scenario to our benchmark

	α	$m_{3/2}$ (TeV)	$\tan\beta$	n
MMAMSB	4.8	21	10	0.5
7 TeV and 10 fb⁻¹				
I	$4.8^{+33.5}_{-1.4}$	22^{+19}_{-21}	9^{+48}_{-8}	$0.5^{+0.5}_{-0.5}$
I + rates	$4.99^{+0.15}_{-0.42}$	$20.0^{+2.9}_{-1.0}$	15^{+10}_{-10}	$0.56^{+0.02}_{-0.10}$
14 TeV and 1 fb⁻¹				
I	$4.8^{+41.0}_{-0.8}$	22^{+15}_{-21}	9^{+48}_{-7}	$0.5^{+0.5}_{-0.1}$
I + rates	$4.80^{+0.31}_{-0.13}$	$21.0^{+1.5}_{-2.1}$	10^{+9}_{-4}	$0.50^{+0.08}_{-0.02}$
14 TeV and 10 fb⁻¹				
I	$4.8^{+0.5}_{-0.6}$	21^{+10}_{-5}	12^{+44}_{-9}	$0.50^{+0.09}_{-0.05}$
I + rates	$4.80^{+0.26}_{-0.12}$	$21.0^{+1.5}_{-1.9}$	10^{+9}_{-3}	$0.50^{+0.07}_{-0.01}$
I + II	$4.80^{+0.07}_{-0.05}$	$21.0^{+1.2}_{-1.3}$	$10.0^{+0.4}_{-0.3}$	$0.500^{+0.005}_{-0.004}$
I + II + rates	$4.80^{+0.04}_{-0.04}$	$21.0^{+0.7}_{-0.7}$	$10.0^{+0.4}_{-0.3}$	$0.500^{+0.005}_{-0.004}$
14 TeV and 100 fb⁻¹				
I	$4.8^{+0.3}_{-0.4}$	21^{+5}_{-4}	10^{+47}_{-4}	$0.50^{+0.09}_{-0.02}$
I + rates	$4.80^{+0.24}_{-0.12}$	$21.0^{+1.5}_{-1.6}$	10^{+7}_{-3}	$0.500^{+0.069}_{-0.008}$
I + II	$4.801^{+0.024}_{-0.023}$	$21.0^{+0.5}_{-0.5}$	$9.99^{+0.19}_{-0.19}$	$0.500^{+0.003}_{-0.003}$
I + II + rates	$4.798^{+0.023}_{-0.019}$	$21.0^{+0.4}_{-0.5}$	$10.00^{+0.19}_{-0.19}$	$0.500^{+0.003}_{-0.003}$

Table 5. Fits to MMAMSB parameters for our chosen benchmark point. Fits are done with various sets of observable groups (I and II) and errors (Tab. 3). Fits are also done with and without the rates observables (Tab. 4).

point. In particular we would like to use the χ^2 of the best-fit point to determine if the CMSSM can be ruled out.

We begin by performing the fit for 10 fb⁻¹ at 7 TeV using only the Group I observables and without the information from rates.³ The results of this fit are shown in Tab. 6. We see that the fit has a viable minimum with a χ^2 of just 0.12. In addition, the fit begins

³For these fits the number of measurements is equal to the number of free parameters. Therefore, a perfect fit to the data ($\chi^2 = 0$) should in principle always be possible, but this is not the case, as is shown by the fits at 14 TeV with 10 fb⁻¹ and 100 fb⁻¹ where $\chi^2 = 2.1$ and $\chi^2 = 11.8$ respectively. There are a couple of reasons for this. One is that the Group I observables only measure the wino, bino and first generation sfermion masses. Thus, they only have weak sensitivity to $\tan\beta$ and A_0 and the fit is effectively to only two free parameters. A second reason is that many other constraints are implicitly present in the fit but not formally included in the number of measurements. For example, we require a neutral LSP so that we have a dark matter candidate, consistent electroweak symmetry breaking, and no tachyonic degrees of freedom. All of these constrain the areas of parameter space that we are able to search to satisfy the mass-edge conditions.

CMSSM	m_0 (GeV)	$m_{1/2}$ (GeV)	$\tan\beta$	A_0 (GeV)	$\chi^2/\text{d.o.f.}$
7 TeV and 10 fb⁻¹					
I	36_{-21}^{+189}	210_{-58}^{+12}	5_{-3}^{+40}	405_{-1056}^{+1256}	0.12/0
I + rates	78	413	7.8	649	216/2
14 TeV and 1 fb⁻¹					
I	35_{-12}^{+59}	208_{-21}^{+10}	$4_{-1.0}^{+29}$	409_{-1038}^{+1237}	0.23/0
I + rates	69	379	7.6	580	334/2
14 TeV and 10 fb⁻¹					
I	$35.3_{-4.8}^{+47.8}$	$208.4_{-10.1}^{+3.2}$	5_{-2}^{+27}	373_{-742}^{+801}	2.1/0
I + rates	59	331	9.4	538	1643/2
I + II	39	210	8.0	364	122/7
I + II + rates	57	328	6.5	531	1806/9
14 TeV and 100 fb⁻¹					
I	$33.6_{-2.1}^{+2.5}$	$207.3_{-2.4}^{+2.1}$	$4.7_{-1.2}^{+2.2}$	365_{-105}^{+112}	11.8/0
I + rates	51	319	8.0	542	2533/2
I + II	38	203	8.1	354	907/7
I + II + rates	173	311	5.8	502	4043/9

Table 6. Best fit points for the CMSSM and the minimum χ^2 for that point and associated set of observables. We only include the 1- σ environment when the best fit point is not excluded at the 99.9% confidence level. We see that rates are extremely effective at ruling out the CMSSM.

to constrain the parameter $m_{1/2}$ ($160 < m_{1/2} < 220$) while the other parameters can vary quite freely, as is illustrated in Fig. 10. As we move to 1 fb⁻¹ at 14 TeV but keep the same observable set, constraints begin to appear on m_0 ($0 < m_0 < 100$) and we still have a minimum where all the observables are well fitted ($\chi^2 = 0.23$).

If we add the rate information to the fit, however, the result changes spectacularly and the best fit has $\chi^2 = 216$ which means that the point is completely excluded by the data. If we examine the individual measurements at this best fit point more closely, we see that the exclusion is dominated by two measurements. The jet-lepton high invariant mass edge, whose true value is $m_{ql}^{\text{high}} = 652$ GeV, has a measured value of 311.9 GeV at the best-fit point, a full 13 σ away. The event rate at the best fit point, $R_{jjE_T^{\text{miss}}} = 231$ fb (measured = 113 fb), is 5.3 σ away. Essentially, the CMSSM model cannot replicate the more compressed mass spectrum with the relatively large masses for the gluino and squarks. The edge observables (especially the difference between the squark and slepton mass) are trying to pull the mass scale down, while the rate observables try to pull the mass scale

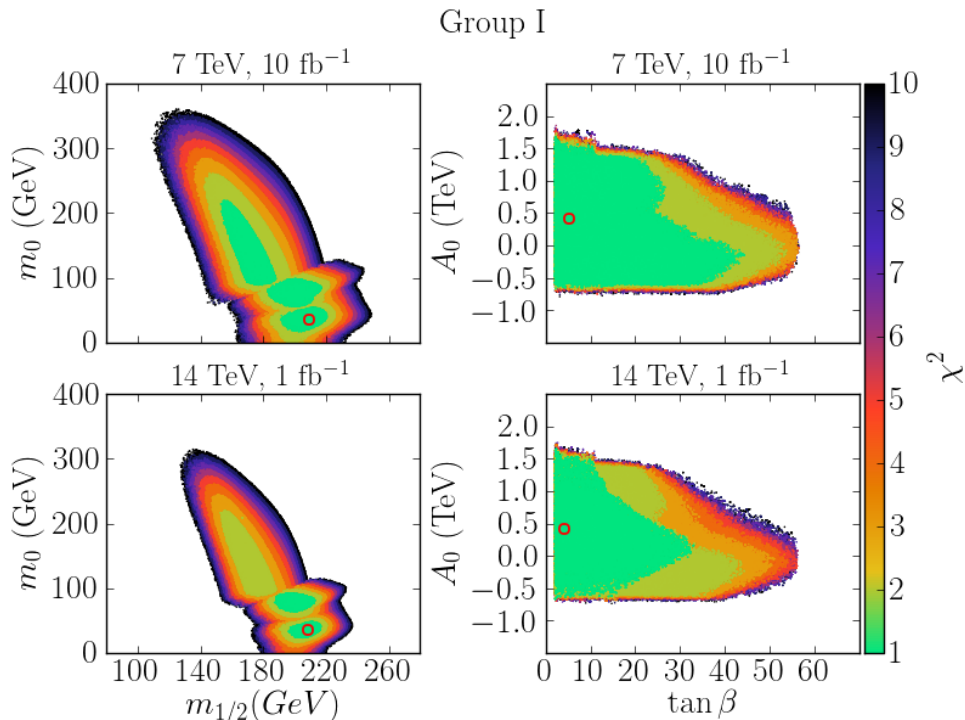


Figure 10. Plots showing the fit of the CMSSM to our MMAMSB benchmark point using only Group I observables and no rate information. The fits in the upper row are for 7 TeV, 10 fb⁻¹ while the bottom row shows the fits for 14 TeV, 1 fb⁻¹.

up. The tension between these two observables leads to the exclusion.

We can also examine the best-fit point found using the Group I mass edges alone to see what rates are predicted for these points. We find that for the best-fit point with 10 fb⁻¹ at 7 TeV, $R_{jjE_T^{\text{miss}}} = 14809$ (measured = 113) and is 652 σ away! Incidentally, this best fit point is already easily ruled out by current searches [5, 7, 12, 13].

Moving to the fits performed at 14 TeV with 10 fb⁻¹, we see that using the Group I observables alone, $\chi^2 = 2.1$, and thus the fit still has a viable minimum. If we add the Group II observables, however, the best-fit point now has a $\chi^2/\text{d.o.f.} = 122/7$ and is thus excluded. The exclusion is dominated by the transverse mass observable, which at the best-fit point is $m_{\tilde{q}}^{T2} = 444$ GeV, 8.9 σ away from the measured value $m_{\tilde{q}}^{T2} = 699$ GeV. The transverse mass is effective as its rough dependence is $m_{\tilde{q}}^{T2} \propto \sqrt{m_{\tilde{q}}^2 - 2m_{\tilde{\chi}_1^0}^2}$ and thus with heavy squarks, it is essentially measuring the squark mass. This leads to a similar tension as in the fits with rates: the transverse mass tries to pull the mass scale of the fit up while the mass edges try to bring the scale down.

Even though the exclusion due to the transverse mass seems convincing, we should compare this to the exclusion that would be achieved by using the rate observables. At the best-fit point, the inclusive rate has the predicted value $R_{jjE_T^{\text{miss}}} = 125$ pb, which is a huge 218 σ away from the value $R_{jjE_T^{\text{miss}}} = 2.78$ pb that would be measured. Thus we can see that the rates are far more effective observables for determining the overall mass scale of a

mAMSB	m_0 (GeV)	$m_{3/2}$ (TeV)	$\tan\beta$	$\chi^2/\text{d.o.f.}$
7 TeV and 10 fb⁻¹				
I	127^{+14}_{-21}	$15.2^{+1.2}_{-1.8}$	21^{+2}_{-19}	3.8/1
I + rates	317	32	33	238/3
14 TeV and 1 fb⁻¹				
I	127^{+10}_{-16}	$15.2^{+0.8}_{-1.4}$	21^{+2}_{-10}	7.6/1
I + rates	316	32	4.7	397/3
14 TeV and 10 fb⁻¹				
I	124	15	21	72/1
I + rates	316	32	25	3084/3
I + II	116	14	16	330/8
I + II + rates	316	32	9	4135/10
14 TeV and 100 fb⁻¹				
I	126	15	21	275/1
I + rates	292	30	11	4591/3
I + II	100	13	16	1886/8
I + II + rates	292	30	9	13678/10

Table 7. Best fit points for the mAMSB and the minimum χ^2 for that point and associated set of observables. We only include the 1- σ environment when the best fit point is not excluded at the 99.9% confidence level. We see that rates are extremely effective at ruling out the mAMSB.

model than the transverse mass is. This can also be seen by comparing the fit done with 10 fb⁻¹ at 7 TeV with only the Group I observables and including rates with the fit done with 10 fb⁻¹ at 14 TeV with Group I and II observables but no rate information. From Tab. 6, we see that even though the fit with rates is done with fewer observables in total and far less data, with a total $\chi^2 = 216$ it more convincingly rules out the CMSSM model than the Group II fit (total $\chi^2 = 122$) that would take at least a few years longer.

5.3 mAMSB

In the previous section we have shown that the MMAMSB can be convincingly distinguished from the CMSSM even with early LHC data (10 fb⁻¹ at 7 TeV). We now do a similar analysis with a different SUSY breaking scenario, mAMSB, to see if the LHC can perform the same task and also separate this model. The mAMSB scenario nearly corresponds to pure anomaly mediation, i.e. the $\alpha \rightarrow 0$ limit of the MMAMSB. As mentioned earlier, however, pure anomaly mediation leads to tachyonic slepton masses. In minimal AMSB (mAMSB), this problem is solved with the addition of a constant contribution m_0

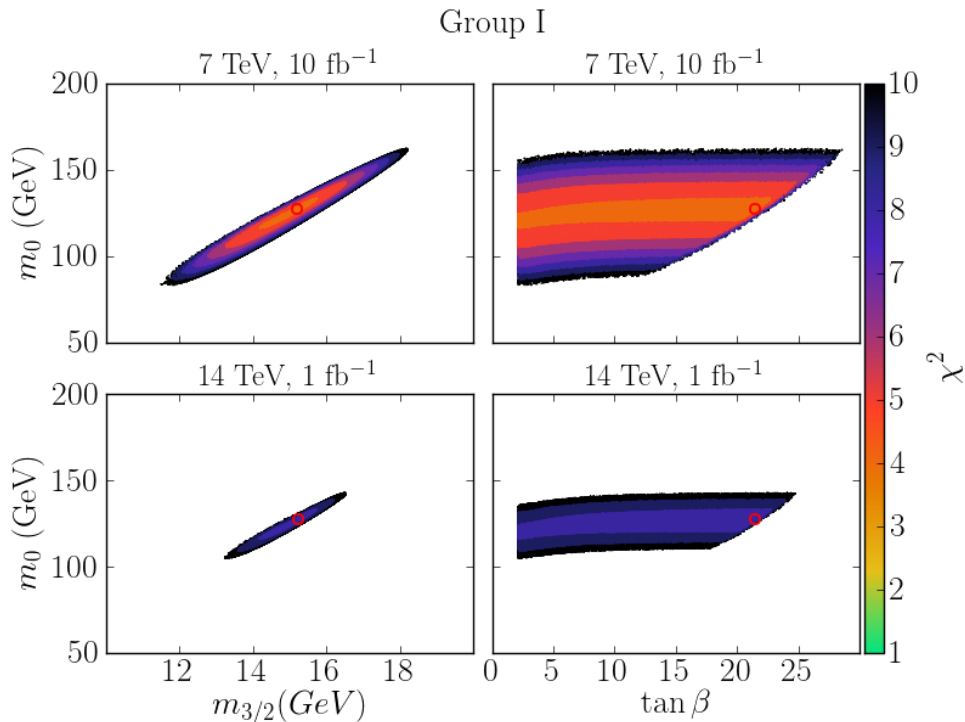


Figure 11. Plots showing the fit of mAMSB to our MMAMSB benchmark point using only Group I observables and no rate information. The fits in the upper row are for 7 TeV, 10 fb⁻¹ while the bottom row shows the fits for 14 TeV, 1 fb⁻¹.

to the scalar masses at the GUT scale. Since $\alpha = 0$ means that the n -dependence in the model also disappears, mAMSB has only three parameters, m_0 , $m_{3/2}$, and $\tan \beta$.

We begin by performing the fit with only the Group I observables at 10 fb⁻¹ at 7 TeV. The results of this fit are shown in the upper row of Fig. 11. The fit has a viable minimum, but a $\chi^2/\text{d.o.f.} = 3.8/1$. Even with just these four mass edge observables and early data, the model already suffers from a little tension. In addition, both m_0 ($100 < m_0 < 150$ GeV) and $m_{3/2}$ ($13.4 < m_{3/2} < 16.4$ TeV) are already relatively constrained. As we move to 1 fb⁻¹ at 14 TeV, the tension in the fit increases and the minimum now has a $\chi^2/\text{d.o.f.} = 7.6/1$. This corresponds to a p-value of less than 0.01 and shows the model is already highly disfavoured. The reason why the Group I observables alone can exclude the model is that the mAMSB contains a larger mass splitting between the gaugino masses than either MMAMSB or the CMSSM (see Sec. 3).

If we include the rates in the fit, however, the exclusion of the model becomes far clearer, as can be seen in the lower row of Fig. 11. Including the event rates with 10 fb⁻¹ at 7 TeV leads to a best fit point with a minimum $\chi^2/\text{d.o.f.} = 238/3$ and the model is completely ruled out. The reason is the same as for the CMSSM: to fit the mass edges requires the mass scale in mAMSB to be low. For example, the masses of all the coloured particles in the best fit point of the Group I fit with 10 fb⁻¹ at 7 TeV are under 400 GeV and the event rates are far higher than they are for the model we are fitting to. This

analysis is confirmed when we look at the individual observables. At the best fit point the jet-lepton high invariant mass edge has the value $m_{q\ell}^{\text{high}} = 653$ GeV, which is 13σ away from its value (312 GeV) at the MMAMSB benchmark point, and is trying pull the mass scale down. On the other hand, the event rate at the best fit point, $R_{jjE_T^{\text{miss}}} = 240$ fb, is 5.7σ away from the MMAMSB value of 113 fb and is trying to pull the mass scale up. The tension between the two observables leads to the clear exclusion.

As for the fit to the CMSSM, we can also examine the effect of the Group II observables on the exclusion and in particular the squark transverse mass, $M_{\tilde{q}}^{T2}$, which is sensitive to the mass scale. We find the fit with Group I and II observables but without event rates with 10 fb^{-1} at 14 TeV has $\chi^2/\text{d.o.f.} = 330/8$ and thus excludes the model. As expected, the exclusion is dominated by $M_{\tilde{q}}^{T2}$ which is 12σ away from the true value at the best fit point. Once again, we have a tension between the edge observables, which are trying to pull the mass scale down, and $M_{\tilde{q}}^{T2}$, which is trying to pull the mass scale up.

In the CMSSM fit, we also compared the effectiveness of the squark transverse mass observable with that of the event rates. Here we do the same by taking the above best fit point with just Group I and II observables and examining what the event rate would be at this point. We find that the event rate $R_{jjE_T^{\text{miss}}} = 539$ pb for the best fit point which is 953σ away from the value (2.78 pb) in our MMAMSB benchmark scenario. Again, this confirms that rates are far more sensitive to the mass scale than $m_{\tilde{q}}^{T2}$ and provide a much more constraining test of the SUSY breaking scenario.

6 Discussion

In the MMAMSB both modulus and anomaly mediated terms can contribute at roughly equal levels to SUSY breaking. This model can have very similar phenomenology to the widely studied CMSSM and mAMSB models. A unique feature of the MMAMSB, however, is that depending on the value of the phenomenological parameter α , the ratio of gaugino masses can be very different from other SUSY breaking scenarios.

In this paper we determined how well we can expect the MMAMSB model to be measured at the LHC and if it is possible to distinguish it from other SUSY breaking scenarios. We fit the model to various hypothetical LHC measurements to see how precisely the input parameters can be determined. Among the inputs to the fits, we included the widely studied mass edges of various SUSY cascade decay chains, as well as other kinematical observables and measurements of ratios of branching ratios that are expected to be possible at the LHC. Special to our procedure, we also included event rate observables, to try and further constrain the model parameters. Event rates are extremely sensitive to the mass scale of the model but are conventionally difficult to include in fits due to the computationally intensive task of running a Monte Carlo event generator for each point in the fit. This is solved by using a combination of cross-section grids and analytically calculated acceptances that is vastly quicker [25].

Using a particular MMAMSB benchmark scenario we showed that the parameters of the model will be difficult to reconstruct with early data if only mass edge measurements are used. When including the event-rate information, however, even early LHC data is

sufficient to constrain the model, especially the parameters that determine the overall mass scale. With more data and more intricate observables, we showed that all the model parameters can be reconstructed with high accuracy ($\lesssim 5\%$).

In addition to showing that the MMAMSB model can be reconstructed, we also demonstrated that it can be distinguished from the CMSSM and the mAMSB. Using only the basic ‘Group I’ mass edges (see Sec. 4), we saw that even with 100 fb^{-1} , it is difficult to conclusively exclude the CMSSM from being able to fit our MMAMSB benchmark point. With the addition of event-rate information, however, the CMSSM interpretation is comprehensively excluded with just 10 fb^{-1} at 7 TeV. We reached a similar conclusion when trying to fit the mAMSB to our benchmark point. Again, when we included rates, the model was easily excluded with early LHC data.

We have seen that rates play a crucial role in measuring and distinguishing different SUSY models. The models considered in this paper have few free parameters. Therefore an obvious direction for future work is to investigate more general models and see if rate information can allow the precise determination of some or all of their parameters.

Acknowledgments

The authors wish to thank Peter Wienemann for all his help in matters relating to `Fittino`. For particular help with including event rates into our fit we would like to thank both Ben O’Leary and Jonas Lindert. In addition, we would like to thank Hans-Peter Nilles for an introduction to the MMAMSB and related discussions. We would also like to acknowledge the help of Kiwoon Choi and Valeri Löwen.

This work has been supported in part by the Helmholtz Alliance ‘Physics at the Terascale’ and the DFG SFB/TR9 “Computational Particle Physics”. HD and JC were supported by BMBF Verbundprojekt HEP-Theorie under the contract 0509PDE.

References

- [1] **ATLAS** Collaboration, G. Aad et al., *Search for supersymmetry using final states with one lepton, jets, and missing transverse momentum with the ATLAS detector in $\sqrt{s} = 7 \text{ TeV}$ pp* , *Phys.Rev.Lett.* **106** (2011) 131802, [[arXiv:1102.2357](#)].
- [2] **ATLAS** Collaboration, G. Aad et al., *Search for squarks and gluinos using final states with jets and missing transverse momentum with the ATLAS detector in $\sqrt{s} = 7 \text{ TeV}$ proton-proton collisions*, *Phys.Lett.* **B701** (2011) 186–203, [[arXiv:1102.5290](#)].
- [3] **ATLAS** Collaboration, G. Aad et al., *Search for supersymmetry in pp collisions at $\sqrt{s} = 7 \text{ TeV}$ in final states with missing transverse momentum and b -jets*, [[arXiv:1103.4344](#)].
- [4] **ATLAS** Collaboration, G. Aad et al., *Search for supersymmetric particles in events with lepton pairs and large missing transverse momentum in $\sqrt{s} = 7 \text{ TeV}$ proton-proton collisions with the ATLAS experiment*, [[arXiv:1103.6214](#)].
- [5] **ATLAS** Collaboration, *Search for supersymmetry with jets, missing transverse momentum and one lepton at $\sqrt{s} = 7 \text{ TeV}$* , Tech. Rep. ATLAS-CONF-2011-090, CERN, Geneva, Jun, 2011.

- [6] **ATLAS** Collaboration, *Search for supersymmetry in pp collisions at $\sqrt{s} = 7\text{TeV}$ in final states with missing transverse momentum, b-jets and no leptons with the atlas detector*, Tech. Rep. ATLAS-CONF-2011-098, CERN, Geneva, Jul, 2011.
- [7] **ATLAS** Collaboration, *Search for supersymmetry in jet(s) plus missing transverse momentum final states with the atlas detector*, Jul, 2011.
- [8] **CMS** Collaboration, *Search for new physics with same-sign isolated dilepton events with jets and missing energy*, Tech. Rep. CMS-PAS-SUS-11-010, Jul, 2011.
- [9] **CMS** Collaboration, S. Chatrchyan et al., *Search for Supersymmetry in pp Collisions at $\sqrt{s} = 7\text{ TeV}$ in Events with Two Photons and Missing Transverse Energy*, *Phys. Rev. Lett.* **106** (2011) 211802, [[arXiv:1103.0953](#)].
- [10] **CMS** Collaboration, S. Chatrchyan et al., *Search for supersymmetry in events with a lepton, a photon, and large missing transverse energy in pp collisions at $\sqrt{s} = 7\text{ TeV}$* , *JHEP* **1106** (2011) 093, [[arXiv:1105.3152](#)].
- [11] **CMS** Collaboration, S. Chatrchyan et al., *Search for Supersymmetry in Events with b Jets and Missing Transverse Momentum at the LHC*, *JHEP* **1107** (2011) 113, [[arXiv:1106.3272](#)].
- [12] **CMS** Collaboration, S. Chatrchyan et al., *Inclusive search for squarks and gluinos in pp collisions at $\sqrt{s} = 7\text{ TeV}$* , [arXiv:1107.1279](#).
- [13] **CMS** Collaboration, S. Chatrchyan et al., *Search for supersymmetry in pp collisions at $\sqrt{s} = 7\text{ TeV}$ in events with a single lepton, jets, and missing transverse momentum*, [arXiv:1107.1870](#).
- [14] I. Hinchliffe, F. Paige, M. Shapiro, J. Soderqvist, and W. Yao, *Precision SUSY measurements at CERN LHC*, *Phys.Rev.* **D55** (1997) 5520–5540, [[hep-ph/9610544](#)].
- [15] B. Allanach, C. Lester, M. A. Parker, and B. Webber, *Measuring sparticle masses in nonuniversal string inspired models at the LHC*, *JHEP* **0009** (2000) 004, [[hep-ph/0007009](#)].
- [16] B. Gjelsten, D. Miller, and P. Osland, *Measurement of SUSY masses via cascade decays for SPS 1a*, *JHEP* **0412** (2004) 003, [[hep-ph/0410303](#)].
- [17] **LHC/LC Study Group** Collaboration, G. Weiglein et al., *Physics interplay of the LHC and the ILC*, *Phys.Rept.* **426** (2006) 47–358, [[hep-ph/0410364](#)].
- [18] C. G. Lester, M. A. Parker, and M. J. White, *Determining SUSY model parameters and masses at the LHC using cross-sections, kinematic edges and other observables*, *JHEP* **0601** (2006) 080, [[hep-ph/0508143](#)].
- [19] P. Bechtle, K. Desch, M. Uhlenbrock, and P. Wienemann, *Constraining SUSY models with Fittino using measurements before, with and beyond the LHC*, *Eur.Phys.J.* **C66** (2010) 215–259, [[arXiv:0907.2589](#)].
- [20] C. Adam, J.-L. Kneur, R. Lafaye, T. Plehn, M. Rauch, et al., *Measuring Unification*, *Eur.Phys.J.* **C71** (2011) 1520, [[arXiv:1007.2190](#)].
- [21] G. Bertone, D. Cerdeno, M. Fornasa, R. de Austri, C. Strege, et al., *Global fits of the cMSSM including the first LHC and XENON100 data*, [arXiv:1107.1715](#).
- [22] O. Buchmueller, R. Cavanaugh, D. Colling, A. De Roeck, M. Dolan, et al., *Supersymmetry and Dark Matter in Light of LHC 2010 and Xenon100 Data*, [arXiv:1106.2529](#).
- [23] B. Allanach and M. J. Dolan, *Supersymmetry With Prejudice: Fitting the Wrong Model to LHC Data*, [arXiv:1107.2856](#).

- [24] G. Corcella, I. Knowles, G. Marchesini, S. Moretti, K. Odagiri, et al., *HERWIG 6: An Event generator for hadron emission reactions with interfering gluons (including supersymmetric processes)*, *JHEP* **0101** (2001) 010, [[hep-ph/0011363](#)].
- [25] H. K. Dreiner, M. Krämer, J. M. Lindert, and B. O’Leary, *SUSY parameter determination at the LHC using cross sections and kinematic edges*, *JHEP* **1004** (2010) 109, [[arXiv:1003.2648](#)].
- [26] P. Bechtle, K. Desch, and P. Wienemann, *Fittino, a program for determining MSSM parameters from collider observables using an iterative method*, *Comput.Phys.Commun.* **174** (2006) 47–70, [[hep-ph/0412012](#)].
- [27] W. Beenakker, R. Höpker, and M. Spira, *PROSPINO: A program for the PROduction of Supersymmetric Particles In Next-to-leading Order QCD*, [hep-ph/9611232](#).
- [28] S. Kachru, R. Kallosh, A. D. Linde, and S. P. Trivedi, *De Sitter vacua in string theory*, *Phys.Rev.* **D68** (2003) 046005, [[hep-th/0301240](#)].
- [29] K. Choi and H. P. Nilles, *The Gaugino code*, *JHEP* **0704** (2007) 006, [[hep-ph/0702146](#)].
- [30] K. Choi, A. Falkowski, H. P. Nilles, M. Olechowski, and S. Pokorski, *Stability of flux compactifications and the pattern of supersymmetry breaking*, *JHEP* **0411** (2004) 076, [[hep-th/0411066](#)].
- [31] K. Choi, A. Falkowski, H. P. Nilles, and M. Olechowski, *Soft supersymmetry breaking in KKLT flux compactification*, *Nucl.Phys.* **B718** (2005) 113–133, [[hep-th/0503216](#)].
- [32] K. Choi, K. S. Jeong, and K. Okumura, *Phenomenology of mixed modulus-anomaly mediation in fluxed string compactifications and brane models*, *JHEP* **0509** (2005) 039, [[hep-ph/0504037](#)].
- [33] A. Falkowski, O. Lebedev, and Y. Mambrini, *SUSY phenomenology of KKLT flux compactifications*, *JHEP* **0511** (2005) 034, [[hep-ph/0507110](#)].
- [34] M. Endo, M. Yamaguchi, and K. Yoshioka, *A Bottom-up approach to moduli dynamics in heavy gravitino scenario: Superpotential, soft terms and sparticle mass spectrum*, *Phys.Rev.* **D72** (2005) 015004, [[hep-ph/0504036](#)].
- [35] H. Baer, E.-K. Park, X. Tata, and T. T. Wang, *Collider and Dark Matter Searches in Models with Mixed Modulus-Anomaly Mediated SUSY Breaking*, *JHEP* **0608** (2006) 041, [[hep-ph/0604253](#)].
- [36] H. Baer, E.-K. Park, X. Tata, and T. T. Wang, *Measuring Modular Weights in Mirage Unification Models at the LHC and ILC*, *Phys.Lett.* **B641** (2006) 447–451, [[hep-ph/0607085](#)].
- [37] W. Cho, Y. Kim, K. Lee, C. Park, and Y. Shimizu, *LHC Signature of Mirage Mediation*, *JHEP* **0704** (2007) 054, [[hep-ph/0703163](#)].
- [38] H. Baer, E.-K. Park, X. Tata, and T. T. Wang, *Collider and Dark Matter Phenomenology of Models with Mirage Unification*, *JHEP* **0706** (2007) 033, [[hep-ph/0703024](#)].
- [39] B. Altunkaynak, B. D. Nelson, L. L. Everett, I.-W. Kim, and Y. Rao, *Phenomenological Implications of Deflected Mirage Mediation: Comparison with Mirage Mediation*, *JHEP* **1005** (2010) 054, [[arXiv:1001.5261](#)].
- [40] F. E. Paige, S. D. Protopopescu, H. Baer, and X. Tata, *ISAJET 7.69: A Monte Carlo event generator for pp, anti-p p, and e+e- reactions*, [hep-ph/0312045](#).
- [41] A. Arbey and F. Mahmoudi, *SuperIso Relic: A Program for calculating relic density and*

- flavor physics observables in Supersymmetry*, *Comput.Phys.Commun.* **181** (2010) 1277–1292, [[arXiv:0906.0369](#)].
- [42] G. Belanger, F. Boudjema, P. Brun, A. Pukhov, S. Rosier-Lees, et al., *Indirect search for dark matter with micrOMEGAs2.4*, *Comput.Phys.Commun.* **182** (2011) 842–856, [[arXiv:1004.1092](#)].
- [43] G. Belanger, F. Boudjema, A. Pukhov, and A. Semenov, *micrOMEGAs: Version 1.3*, *Comput.Phys.Commun.* **174** (2006) 577–604, [[hep-ph/0405253](#)].
- [44] G. Belanger, F. Boudjema, A. Pukhov, and A. Semenov, *MicrOMEGAs: A Program for calculating the relic density in the MSSM*, *Comput.Phys.Commun.* **149** (2002) 103–120, [[hep-ph/0112278](#)].
- [45] P. Bechtle, O. Brein, S. Heinemeyer, G. Weiglein, and K. E. Williams, *HiggsBounds 2.0.0: Confronting Neutral and Charged Higgs Sector Predictions with Exclusion Bounds from LEP and the Tevatron*, [arXiv:1102.1898](#).
- [46] B. Allanach, M. Battaglia, G. Blair, M. S. Carena, A. De Roeck, et al., *The Snowmass points and slopes: Benchmarks for SUSY searches*, *Eur.Phys.J.* **C25** (2002) 113–123, [[hep-ph/0202233](#)].
- [47] **WMAP** Collaboration, E. Komatsu et al., *Five-Year Wilkinson Microwave Anisotropy Probe (WMAP) Observations: Cosmological Interpretation*, *Astrophys.J.Suppl.* **180** (2009) 330–376, [[arXiv:0803.0547](#)].
- [48] **XENON100** Collaboration, E. Aprile et al., *Dark Matter Results from 100 Live Days of XENON100 Data*, *Phys.Rev.Lett.* (2011) [[arXiv:1104.2549](#)].
- [49] S. AbdusSalam, B. Allanach, H. Dreiner, J. Ellis, U. Ellwanger, et al., *Benchmark Models, Planes, Lines and Points for Future SUSY Searches at the LHC*, [arXiv:1109.3859](#). *
Temporary entry *.
- [50] W. Beenakker, R. Höpker, M. Spira, and P. Zerwas, *Squark and gluino production at hadron colliders*, *Nucl.Phys.* **B492** (1997) 51–103, [[hep-ph/9610490](#)].
- [51] W. Beenakker, M. Kramer, T. Plehn, M. Spira, and P. Zerwas, *Stop production at hadron colliders*, *Nucl.Phys.* **B515** (1998) 3–14, [[hep-ph/9710451](#)].
- [52] S. Gieseke et al., *Herwig++ 2.5 Release Note*, [arXiv:1102.1672](#).
- [53] M. Bahr et al., *Herwig++ Physics and Manual*, *Eur. Phys. J.* **C58** (2008) 639–707, [[arXiv:0803.0883](#)].
- [54] A. Buckley, J. Butterworth, L. Lonnblad, H. Hoeth, J. Monk, et al., *Rivet user manual*, [arXiv:1003.0694](#).
- [55] M. Cacciari and G. P. Salam, *Dispelling the N^3 myth for the k_t jet-finder*, *Phys. Lett.* **B641** (2006) 57–61, [[hep-ph/0512210](#)].
- [56] M. Cacciari, G. P. Salam, and G. Soyez, *The anti- k_t jet clustering algorithm*, *JHEP* **04** (2008) 063, [[arXiv:0802.1189](#)].
- [57] C. Lester and D. Summers, *Measuring masses of semiinvisibly decaying particles pair produced at hadron colliders*, *Phys.Lett.* **B463** (1999) 99–103, [[hep-ph/9906349](#)].
- [58] A. Barr, C. Lester, and P. Stephens, *$m(T2)$: The Truth behind the glamour*, *J.Phys.G* **G29** (2003) 2343–2363, [[hep-ph/0304226](#)].

- [59] B. K. Gjelsten, D. J. Miller, and P. Osland, *Resolving ambiguities in mass determinations at future colliders*, [hep-ph/0507232](#).
- [60] B. K. Gjelsten, D. J. Miller, P. Osland, and A. R. Raklev, *Mass ambiguities in cascade decays*, [hep-ph/0611080](#).
- [61] H.-U. Martyn, *Study of sleptons at a linear collider - supersymmetry scenario SPS 1a*, [hep-ph/0406123](#).
- [62] J. Conley, H. Dreiner, and P. Wienemann, *Measuring a Light Neutralino Mass at the ILC: Testing the MSSM Neutralino Cold Dark Matter Model*, *Phys.Rev.* **D83** (2011) 055018, [[arXiv:1012.1035](#)].